Eur. Phys. J. E **2**, 229–245 (2000)

THE EUROPEAN PHYSICAL JOURNAL E

EDP Sciences
© Società Italiana di Fisica
Springer-Verlag 2000

Electron density modeling and reconstruction of infinite periodic minimal surfaces (IPMS) based phases in lipid-water systems. II. Reconstruction of D surface based phases

P.E. Harper[1,a], S.M. Gruner[1,b], R.N.A.H. Lewis[2], and R.N. McElhaney[2]

[1] Department of Physics, Joseph Henry Laboratories, Jadwin Hall, Princeton University, Princeton NJ 08544, USA
[2] Department of Biochemistry, The University of Alberta, Edmonton, Alberta, Canada T6G 2H7

Received 15 January 1999 and Received in final form 20 October 1999

Abstract. This is the second of two papers dealing with the structure of lipid-water phases based on Infinite Periodic Minimal Surfaces (IPMS). The first paper describes mathematical modeling of such phases. In this paper, a new reconstruction method, called the methyl trough search, is described and used to solve the structures based on powder pattern X-ray diffraction data. Structures are derived for both a single chain lipid-water system (mono-olein) and a diacyl phospholipid-water system (2-2 methyl butyl 16:0 phosphatidylcholine). The methyl trough search uses the low electron density of the lipid methyl tails to determine the correct phasing for the electron density reconstruction. The data are consistent with a structure based on the IPMS D surface. The results are compared to other methods used to solve the mono-olein structure; the structure of the diacyl lipid has never before been solved. We discuss the subtleties involved in reconstruction of D surface based phases and the substantial artifacts that arise in low-resolution reconstructions of hydrocarbon lipids lacking heavy-atom sites.

PACS. 61.30.Cz Theory and models of liquid crystal structure – 87.15.By Structure and bonding – 83.70.Jr Liquid crystals: nematic, cholesteric, smectic, discotic, etc

1 Introduction

Scriven's [1] suggestion that amphiphile structures may be based on Infinite Periodic Minimal Surfaces (IPMS) has led to a great deal of experimental and theoretical interest in lipid phases with cubic symmetries (both recently [2–8] and in the past [9–12]). Because these phases are geometrically complex, only a few groups have attempted to solve the X-ray structures of D surface based systems [13–15]. The solutions which have been derived have not been compared with D surface based models, nor has there been a detailed examination of the bilayer variations in these structures. The most detailed reconstructions performed to date [16] require a reference phase of identical composition and known X-ray phases. In this paper we develop a new structure solution procedure which begins by constructing IPMS-based models of the data for both mono-olein, for which structures have been published, and 2-2 methyl butyl 16:0 phosphatidylcholine, for which there are no published structures. The models and data are then reconstructed using a new phasing procedure, called the methyl trough search, which only requires a single data set. Finally, the structures which are derived are examined by comparing one-dimensional profiles of the bilayer at various points on the structure to the profiles derived from the model. It is found that the D surface based models correspond well to the experimental amplitudes and that the new phasing method is robust and consistent with prior results for mono-olein [15]. (Note: Much of the work presented in this paper may also be found in the Ph.D. thesis of Paul Harper [17].)

Mono-olein was purchased from Sigma Chemical Co. and 2-2 methyl butyl 16:0 phosphatidylcholine (PC) was synthesized [18]. Excess water samples were prepared by adding 3-5 mg lipid and a roughly equal weight of deionized water to a 1.5 mm quartz X-ray capillary. The lipid and water were thoroughly mixed with a 10 microliter Drummond dispenser (Drummond Scientific, Broomhall, PA) and the capillary sealed with epoxy, taking care to leave an air gap of a few mm above the sample so the epoxy did not contact the sample. The samples were equilibrated for over an hour at the measurement temperature.

X-rays were generated by a Rigaku RU-200 rotating anode X-ray machine equipped with a Cu anode operated at a typical loading of 50 kV and 55 mA and a

[a] *Current address*: Department of Physics and Astronomy, Calvin College, 3201 Burton SE, Grand Rapids, MI 49546, USA.
e-mail: pharper@grand-canyon.edu
[b] *Current address*: Physics Department, Cornell University, 162 Clark Hall, Ithaca, NY 14853-2501, USA.
e-mail: smg26@cornell.edu

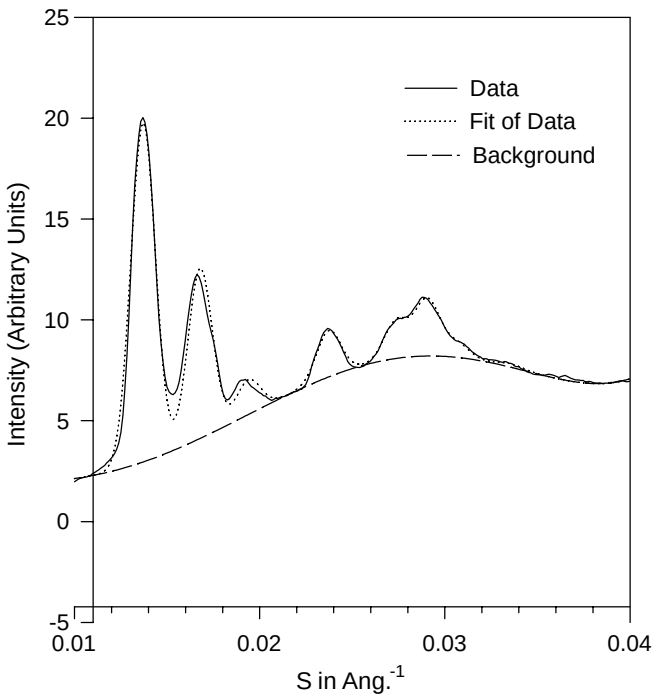

Fig. 1. Plot of scattering intensity for the mono-olein data. The data is shown as a solid line, the background as a dashed line, and the fit as a dotted line.

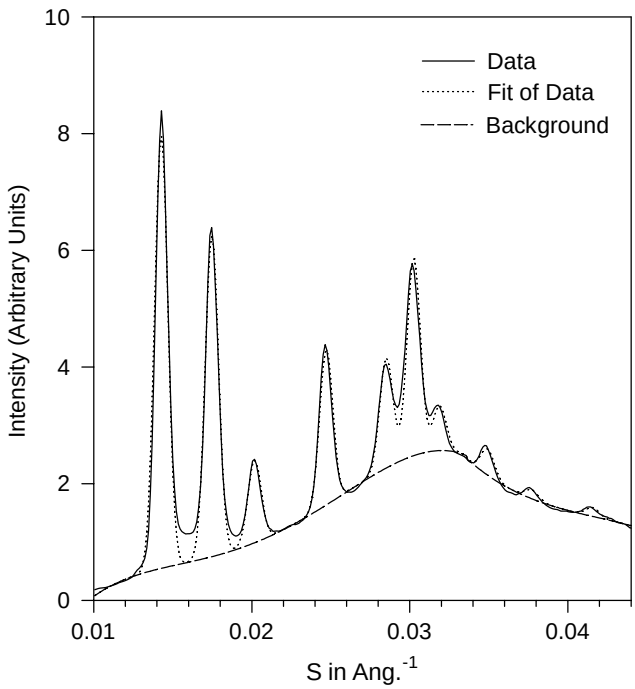

Fig. 2. Plot of scattering intensity for the 2-2 methyl butyl 16:0 PC data. The data is shown as a solid line, the background as a dashed line, and the fit as a dotted line.

0.2 mm × 2 mm microfocus cup, which yields a foreshortened focus at 6 degrees of about $(0.2\,\mathrm{mm})^2$. The X-ray beams were Ni filtered, and focused with a Franks mirror optics and slit collimation. The samples were kept in a temperature regulated stage at 25 °C for mono-olein and at 20 °C for 2-2 methyl butyl 16:0 phosphatidylcholine and the resulting diffraction data was collected by either of two home-built X-ray detectors (*e.g.*, the Intensifier/lens/CCD detector [19] or the SIT detector [20]). Several dozen exposures of 10 minutes with the SIT detector or a few multiple hour exposures with the CCD-based detector were taken and then added together. The resulting powder pattern picture was then azimuthally integrated to produce the plots shown in Figures 1 and 2. The peaks were fit with Gaussians and the background was fit in several sections with polynomials that were constrained to be continuous and smooth across the section boundaries. Ag Stearate (d-spacing 48.68 Å [21]) was used as a calibrant in measuring the unit cell basis length (d-spacing).

2 Space group identification

For the cases studied in this paper, there are enough reflections to make any space group other than Pn$\bar{3}$ or Pn$\bar{3}$m unlikely [13,22]. For instance, cubic space groups of the form Pn..n do not have a $(2,0,0)$ reflection, a reflection that is present in all the samples studied in this paper. The Ia$\bar{3}$d space group (the space group of the gyroid) in which many reflections are extinguished (for example, the $(1,1,0)$, $(1,1,1)$, and $(2,0,0)$ reflections) is excluded because these reflections are present in the data studied. However, one unfortunately cannot distinguish between the Pn$\bar{3}$ and Pn$\bar{3}$m space groups on the basis of powder pattern reflections only. The Pn$\bar{3}$m space group is identical to the Pn$\bar{3}$ space group except for the condition that the amplitudes $F_{hkl} = F_{hlk}$ when $h \neq k \neq l$. Fortunately, the only reflections that have yet been experimentally observed for which this is relevant are the $(3,1,0)$ and $(3,2,1)$ reflections. Given that one does not know the proper partition into F_{hkl} and F_{hlk} for a given powder pattern reflection for which $h \neq k \neq l$, the best guess is to split the reflection evenly between the two amplitudes, which results in Pn$\bar{3}$m symmetry. A truly satisfactory resolution awaits diffraction from a single crystal, in which it would be possible to measure F_{hkl} and F_{hlk} individually.

To avoid possible confusion, it should be noted that there has been a reconstruction of a phase of space group Pm$\bar{3}$n [23]. Despite the similarity of name of this space group and the space group of the D surface (Pn$\bar{3}$m), they are quite different and can be easily distinguished. For example, the (111) reflection, which is quite strong in all the Pn$\bar{3}$m patterns with which the authors are familiar, is extinguished in the Pm$\bar{3}$n space group.

3 Evidence for IPMS-based phases

Besides reconstruction efforts, evidence in support of IPMS-based phases comes from the pulsed field gradient NMR technique [24,25]. Work of this type shows that both lipid and water can diffuse over large distances, which is consistent with an IPMS-based description and rules out structures based entirely on micelles and inverted micelles.

It has also been shown that an IPMS-based description yields bilayer dimensions similar to those seen in lamellar systems [26,27]. Subtler arguments can also be made. The three IPMS studied in this series of papers, the D, G, and P surfaces, are quite similar, as detailed in the first paper [29]. In fact, one can scale the unit cells for each surface so that the bilayer curvatures are identical for each surface (see section 3.2 in previous paper [29]). One can then rank these according to water content, yielding, in order of decreasing water content, P, D, and G. This implies that dehydrating a D surface based system would force a phase transition to a G surface based system, as is in fact quite commonly observed [10]. Additionally, dehydrating a P surface based phase would result in a D surface based phase. One would expect to see the d-spacings at the phase boundaries match so that the bilayer curvatures are the same. This has been found to be the case for several systems, [26,30] and is at least roughly true for a 12 carbon glycerol [11], making for rather interesting and quantitative argument for IPMS-based phases.

4 Brief review of reconstruction efforts

Perhaps the earliest attempt at electron density reconstruction of a D surface based phase was made by Tardieu in her doctoral thesis [28]. However, her results were not published elsewhere. The first published effort appears to have been performed by Longley and McIntosh [13]. These authors made several models of the double diamond phase of mono-olein, the best of which was composed of two interpenetrating diamond lattice networks of rods. The rods were assigned a non-zero electron density and the remainder of the system was assigned an electron density of zero. The electron densities of the model were then Fourier transformed and the resulting amplitudes were compared to the diffraction amplitudes of mono-olein. The model was then adjusted to yield the best agreement with the experimental amplitudes. The phasing from the final model was then used for the reconstruction. Finally, the reconstruction was examined using two-dimensional cuts through the unit cell. Though an important first effort, the approximate nature of the model employed leaves the accuracy of the phasing an open issue. It is also difficult to check the accuracy of a reconstruction *via* two-dimensional cuts and to distinguish anything more than gross features from such plots.

Another effort at reconstructing the double diamond phase of mono-olein is detailed in [14]. In this method, an artificial "entropy" is postulated,

$$S \equiv \int_V \rho(\mathbf{r}) \ln[\rho(\mathbf{r})] \, \mathrm{d}v, \tag{1}$$

where $\rho(\mathbf{r})$ is the absolute electron density and the integral is over the volume of the unit cell [15]. In a certain regime, this "entropy" is maximized when $\langle \Delta\rho^4 \rangle$ is a minimum, where $\Delta\rho$ is the reconstructed electron density. Note that $\Delta\rho \equiv \rho - \rho_{\mathrm{ave}}$, where the average is a volume average over the unit cell. The idea is that the proper phasing yields the maximum "entropy" and hence a minimum $\langle \Delta\rho^4 \rangle$. This method, known as the "maximum entropy" method, has difficulties. It is physically suspect to define a function that contains the logarithm of a quantity that is not dimensionless. Furthermore, the deficiencies of this method have been noted by Mariani [23], in which it is stated that the correct phasing is not necessarily the one for which $\langle \Delta\rho^4 \rangle$ is a minimum. As a result, the phasing result of [14] for the double diamond phase of mono-olein would also be questionable, except for having support *via* the pattern recognition approach, as detailed below.

It is instructive to review the pattern recognition approach which was applied to mono-olein in [15]. (See [23] for a more recent version of this phasing method.) The principle behind the pattern recognition approach is that phases of identical chemical composition should possess the same electron density histograms. One can construct an electron density histogram by dividing the unit cell into a grid and calculating the average electron density in each grid element and making a histogram of the results. For instance, the fraction of the grid elements possessing the density of the phosphorous headgroup should be the same for different phases, so long as the composition stays the same. To put it another way, in a phase transition where the chemical composition stays the same, one is merely rearranging the constituents. As a measure of the similarity of the histograms, they use the moments of the reconstructed electron density, $\langle \Delta\rho^n \rangle$. If one has a known reference phase, one can then find the phasing of an unknown phase of identical composition by picking the phasing that yields the best agreement with the electron density moments of the known reference phase. Finally, the authors of this method used "shape normalization" *via* Gaussian apodization of data. "Shape normalization" means that the curvature of the autocorrelation function at the origin must be the same for both the reference phase and the unknown phase. The curvature of the autocorrelation function at the origin is given by

$$p'' = -\left(\frac{4\pi^2}{3a^2}\right) \frac{\sum_{hkl}(h^2+k^2+l^2)F_{hkl}^2}{\sum_{hkl} F_{hkl}^2}, \tag{2}$$

where p'' is the curvature of the autocorrelation function at the origin, a is the unit cell size, and F_{hkl} are the amplitudes.

An appraisal of the pattern recognition approach requires an understanding of the derivation of equation (2) as follows: One can define the autocorrelation or Patterson function as

$$p(\mathbf{x}) \equiv \frac{1}{V} \int \rho(\mathbf{x}')\rho(\mathbf{x}'+\mathbf{x}) \, \mathrm{d}v', \tag{3}$$

where V is the volume of the unit cell, ρ is the electron density as a function of position, and the integration takes place over the volume of the unit cell. As shown in [31], for centrosymmetric systems this can be converted to

$$p(x,y,z) = \sum_{hkl} F_{hkl}^2 \cos\left[\frac{2\pi}{a}(hx+ky+lz)\right], \tag{4}$$

where F_{hkl} are the amplitudes, h, k, and l are the peak indices, and a is the unit cell size. If one converts the above expression to spherical coordinates, the result is

$$p(r,\theta,\phi) = \sum_{hkl} F_{hkl}^2 \cos\left[\frac{2\pi r}{a}(h\sin\theta\cos\phi + k\sin\theta\sin\phi + l\cos\theta)\right]. \quad (5)$$

For small r, one can expand the cos term, which yields

$$p(r,\theta,\phi) = \sum_{hkl} F_{hkl}^2 \left[1 - \frac{1}{2}\left(\frac{2\pi r}{a}\right)^2 (h\sin\theta\cos\phi + k\sin\theta\sin\phi + l\cos\theta)^2\right]. \quad (6)$$

Next, one can take the spherical average, which is defined to be

$$p(r) = \frac{\int p(r,\theta,\phi)\sin\theta\,\mathrm{d}\theta\,\mathrm{d}\phi}{\int \sin\theta\,\mathrm{d}\theta\,\mathrm{d}\phi}. \quad (7)$$

After evaluating the integrals, one gets

$$p(r) = \sum_{hkl} F_{hkl}^2 \left[1 - \frac{1}{6}\left(\frac{2\pi r}{a}\right)^2 (h^2+k^2+l^2)\right]. \quad (8)$$

The curvature at the origin is calculated by taking the second derivative with respect to r and then evaluated at $r = 0$, which yields, at last,

$$p''(r=0) = \sum_{hkl} F_{hkl}^2 \left(\frac{4\pi^2}{3a^2}\right)(h^2+k^2+l^2). \quad (9)$$

Note that this equation is equivalent to equation (2) when the amplitudes are normalized according to

$$\sum_{hkl} F_{hkl}^2 = 1, \quad (10)$$

which is the standard normalization used by Mariani and Luzatti.

Mariani *et al.* [14] feel justified in modifying the diffraction data to conform to the postulate that the curvature of the autocorrelation function at the origin must be the same for both the reference and unknown phases. This was done *via* Gaussian apodization, *i.e.*,

$$F_{hkl}^{\mathrm{apod}} = F_{hkl} e^{-\beta^2(h^2+k^2+l^2)/a^2}, \quad (11)$$

where F_{hkl} are the original amplitudes, F_{hkl}^{apod} are the apodized amplitudes, hkl are the indices, a is the unit cell size, and β is a free parameter to be adjusted for each phase so that p'' will be identical for each phase. "Shape normalization" is intended to correct for differences in truncation errors in the two phases, a laudable goal. However, it is not at all clear why one is justified in altering the data *via* Gaussian apodization in order to achieve this goal. It is also unclear whether one should apodize one set of data to match the other or whether both should be apodized to meet at a common point [32].

The pattern recognition approach does have a great strength in that it requires no presuppositions about the structure of the unknown phase, though it does present the difficulty of requiring a known reference phase of identical composition and requiring some data manipulation of uncertain justification. Finally, and most importantly, despite the above criticisms, it yields phasings for D surface based phases that are in agreement with the phasing method and modeling developed in this paper.

5 Methyl trough search

Our new phasing technique takes advantage of the fact that the terminal methyl groups of lipid chains have, by far, the lowest electron density of any part of a lipid-water system. If one assumes that the system is based on a minimal surface dividing a bilayer, the methyl trough should lie directly on the minimal surface. One can, therefore, phase a system by searching for the position of the electron density minimum, the methyl trough, and comparing this with the minimal surface position. It should be pointed out that the obvious weakness of this method is that it assumes one has an IPMS-based phase. However, if this method is combined with modeling that yields amplitudes in reasonable agreement with experimental measurements, a good case could be made for these phasing results. In D surface based systems, this search has been implemented by searching for a global minimum along a coordinate axis, arbitrarily labeled the z-axis, at several different points in the unit cell and finding the maximum and root-mean-square deviations from the minimal surface (Fig. 3). In order to reconstruct the systems encountered, it was only necessary to search for minima along lines in the z-direction at six pairs of (x, y) coordinates in the unit cell, namely $(0,0)$, $(0,0.125)$, $(0,0.25)$, $(0.125,0.125)$, $(0.125,0.25)$ and $(0.25,0.25)$ (Fig. 3). Note that due to cubic symmetry, one could equivalently pick any coordinate axis instead of the z-axis. A finer grid is unnecessary, as it would exceed the resolution of the data studied and would be more costly in terms of computing time. Using the above-mentioned grid, it took several hours of computing time on an Intel-486 based 50 MHz computer to phase each system studied in this paper.

The extrema for $\rho(z)$ were found numerically and the one that yielded the lowest electron density was selected. When there were multiple solutions for the lowest electron density, the solution with the lowest z was picked. The position of minimal electron density $z_{\min}$ was found for each search line and compared with the z-coordinate of the minimal surface (z_{surf}) for that line. The difference between these two is defined to be Δ, where

$$\Delta \equiv z_{\min} - z_{\mathrm{surf}}. \quad (12)$$

One then defines $\Delta_{\max}$ to be the maximum of the set of Δ values. It is also useful to define Δ_{rms}, which is the

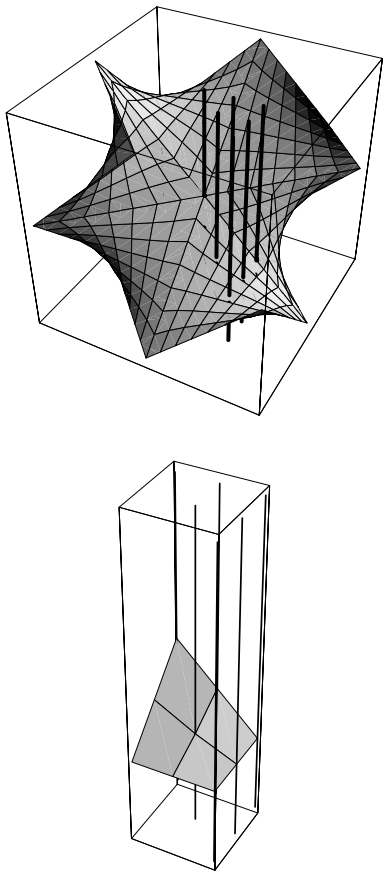

Fig. 3. Top view: unit cell of the D surface. The vertical lines indicate the locations of the electron density minima searches. Bottom view: section of the unit cell pierced by the electron density minima searches.

root mean square of the set of Δ values. It was found that the correct phasing satisfied the criterion $\Delta_{\max} < 0.1$, as $\Delta_{\max}$ values larger than this yielded methyl trough surfaces noticeably deviant from the minimal surface. In fact, the correct phasing yields a methyl trough surface that is practically identical to the minimal surface (Fig. 4). As can be seen in Figure 4, distortion is even observable in some surfaces with $\Delta_{\max} < 0.1$; when $\Delta_{\max}$ exceeds 0.1, the distortion is marked.

6 Model of mono-olein

Mono-olein is a well-studied compound [13,14,26] whose density is 0.9420 gm/ml at 20 °C and molecular weight is 356.6 [33]. Knowing these and assuming a coefficient of volume expansion of $7 \times 10^{-4}/\,°\mathrm{C}$ typical for lipids of this type [34], the volume is calculated to be 631 Å^3 and the density to be 0.9387 gm/ml at 25 °C. In determining the volumes of the individual parts of the lipids, it useful to consider the following formula. The volumes of saturated hydrocarbons fit

$$v_{\text{hydrocarbon}} = N_{\mathrm{CH_2}} \times 26.6\,\text{Å}^3 + N_{\mathrm{CH_3}} \times 56.3\,\text{Å}^3. \quad (13)$$

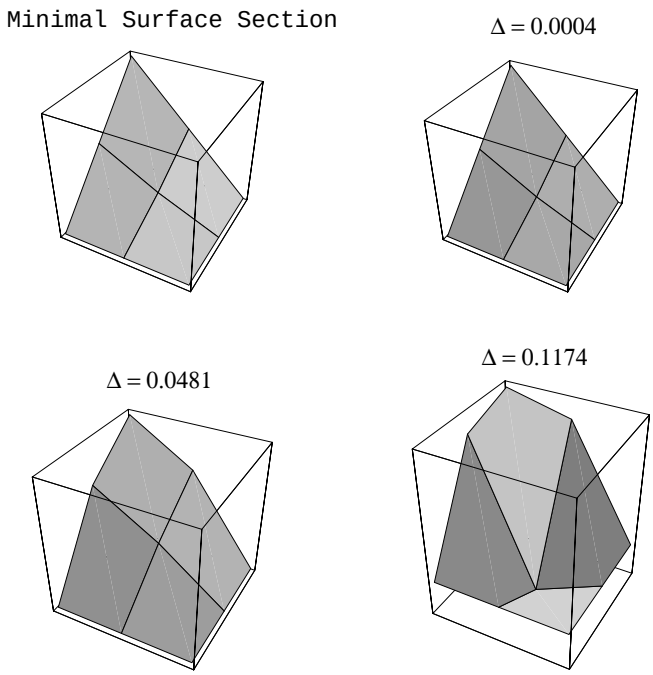

Fig. 4. The top left plot is an actual minimal surface section, with the remaining plots being methyl trough search results for the modeled mono-olein data. The plot on the top right is the methyl trough search result for the correct phasing. $\Delta_{\max}$ is given at the top of each of the methyl trough search plots.

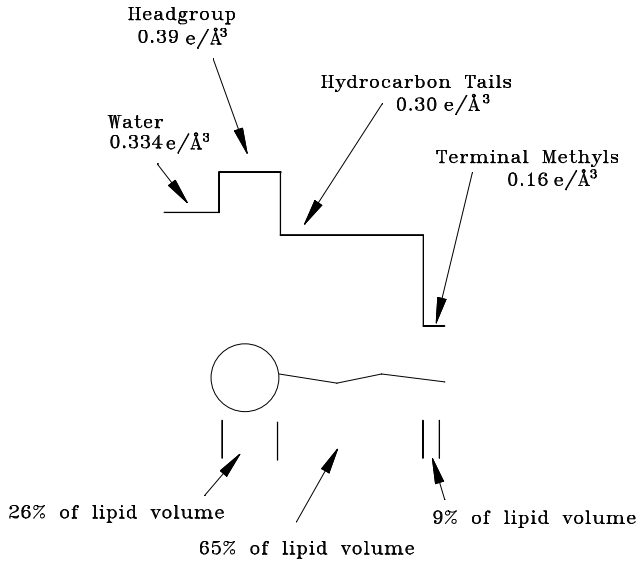

Fig. 5. Electron density model for mono-olein.

From the above formula [17], the terminal methyl occupies 56.3 Å^3 or about 9% of the lipid volume. The volume of the hydrocarbon tail (without the terminal methyl) can be estimated to be

$$v_{\text{tail-methyl}} \cong 16 v_{\mathrm{CH_2}} - v_{\text{n-octane}} + v_{\text{cis-2-octene}}, \quad (14)$$

which results in a volume of 413 Å^3, or 65% of the molecule. The remaining 26% or 162 Å^3 of mono-olein is taken up by the headgroup. The electron density of the

Table 1. The middle three columns contain the Fourier amplitudes for a constant thickness volume with unitary electron density that extends a distance equal to the monolayer thickness from each side of the minimal surface. The monolayer thickness is given in a fraction of a unit cell length (side of a unit cell = 1). Note that $q = (0, 0, 0)$ corresponds to the volume occupied by the constant thickness volume. The final column contains the resulting amplitudes for a model of mono-olein. See [29] for general information on D surface based model construction. See section 6 for the specific details on this model of mono-olein.

Amplitudes for mono-olein model				
q	Monolayer thickness			Bilayer model
	0.0144	0.1226	0.1712	
$(0, 0, 0)$	0.0552	0.4545	0.6143	
$(1, 1, 0)$	0.0137	0.0917	0.0997	−1.00
$(1, 1, 1)$	0.0139	0.0855	0.0849	−1.03
$(2, 0, 0)$	−0.0074	−0.0375	−0.0277	+0.56
$(2, 1, 1)$	0.0061	0.0258	0.0137	−0.45
$(2, 2, 0)$	0.0073	0.0232	0.0035	−0.53
$(2, 2, 1)$	0.0079	0.0217	−0.0012	−0.56
$(3, 1, 0)$	−0.0053	−0.0118	0.0032	+0.35
$(3, 1, 1)$	−0.0028	−0.0051	0.0026	+0.17
$(2, 2, 2)$	0.0082	0.0122	−0.0136	−0.51
$(3, 2, 1)$	0.0027	0.0022	−0.0057	−0.15

headgroup can then be calculated to be $0.36\,\mathrm{e}/\mathrm{Å}^3$, which is, as expected, much lower than the electron density for a phosphorous head group, which is $0.54\,\mathrm{e}/\mathrm{Å}^3$ (see Fig. 5 from [29] for a plot of a strip model for a phospholipid). Using the electron densities for the methyl and hydrocarbon tails, which are, respectively, $0.16\,\mathrm{e}/\mathrm{Å}^3$ and $0.30\,\mathrm{e}/\mathrm{Å}^3$, a strip model for mono-olein can be constructed, as shown in Figure 5. From the outset, note that the methyl tail is the feature with the most contrast, as will be important in the reconstructions.

From [26], it is known that the excess water phase of mono-olein first occurs at a weight fraction of lipid of 0.60 and, hence, a volume fraction of 0.615. The fraction of the unit cell occupied by the methyl groups is then 0.055 and the fraction occupied by the methyl groups and the hydrocarbon tails is 0.46. The appropriate half-thicknesses for the constant thickness volumes bounded by the methyl-tail interface, the tail-headgroup interface, and the headgroup-water interface, are, respectively, 0.0144, 0.1226, and 0.1712. Using the modeling methods developed in [29], the Fourier amplitudes can be calculated for these constant thickness volumes and combined with the electron densities for the relevant components to produce model amplitudes. The calculated Fourier amplitudes and the model amplitudes are shown in Table 1.

7 Reconstruction of mono-olein model

The methyl trough search method works quite well on the mono-olein model, as one might expect, given that the methyl trough is the dominant feature in the electron density profile. The proper phasing for the model system is ranked number one (Tab. 2) and the methyl trough search surface is quite close to the minimal surface (Fig. 4).

At this point, the top phasing combinations for the model system will be examined, as preparation for examining experimental data. The phase rankings for the top phasing combinations are listed in Table 2. The list of possible phasing combinations is cut to the seventeen combinations that satisfy the condition $\Delta_{\max} < 0.1$. To sort through these remaining phases and check the physical reasonableness of the reconstruction, one turns to the cuts defined in section 3.3 of [29] (see Fig. 5 of [29] for the position of the cuts). The electron density values along these cuts are shown individually in Figure 8 of [29]. *In the superposition display of these cuts, which is used throughout this paper, the solid and dashed lines are cuts through the bilayer at the flat point and the point of maximum Gaussian curvature in the minimal surface, respectively.* The flat point is the point at which both the mean curvature and the Gaussian curvature are zero. These give a perspective of the bilayer at the two extremes of curvature; they give one an idea of the range variation in the bilayer over the different parts of the minimal surface. Furthermore, for those familiar with lamellar electron density reconstructions, they give a readily accessible means of evaluating the plausibility of the phasing. These cuts, with the results from the methyl trough search, will be used for all the reconstructions in this paper.

Before utilizing these cuts for phasing efforts, it is instructive to outline the main features of the cuts, as seen in Figure 6. In the center, one sees a deep trough due to the low electron density methyl tails. Moving out in either direction from the center, one next encounters the peak due to the higher electron density headgroups. Ideally, the electron density should then flatten out to the electron density of water, which is intermediate between the headgroup and methyl tail electron densities. However, as seen in the diagram, truncation effects dominate the water region and spurious peaks arise, as is well

Table 2. Methyl trough phasing results for a model mono-olein system. The nine most likely phases are shown, ranked by the value of $\Delta_{\max}$. The correct phasing is marked with an arrow.

Rank	$\Delta_{\max}$	Δ_{rms}	Phasing											
			1	1	2	2	2	2	3	3	2	3	4	3
			1	1	0	1	2	2	1	1	2	2	0	2
			0	1	0	1	0	1	0	1	2	1	0	2
1	0.0004	0.0002	−	−	+	−	−	−	+	+	−	−	0	0 ⇐
2	0.0174	0.0086	−	−	+	−	−	−	+	+	−	+	0	0
3	0.0222	0.0123	−	−	+	+	−	−	+	+	−	−	0	0
4	0.0235	0.0106	−	−	−	−	−	−	+	+	−	−	0	0
5	0.0291	0.0144	−	−	−	−	−	−	+	+	−	+	0	0
6	0.0295	0.0162	−	−	+	−	−	−	−	−	−	−	0	0
7	0.0316	0.0153	−	−	+	−	−	−	+	−	−	−	0	0
8	0.0353	0.0150	−	−	+	−	−	−	−	+	−	−	0	0
9	0.0414	0.0173	−	−	+	−	−	−	+	−	−	+	0	0

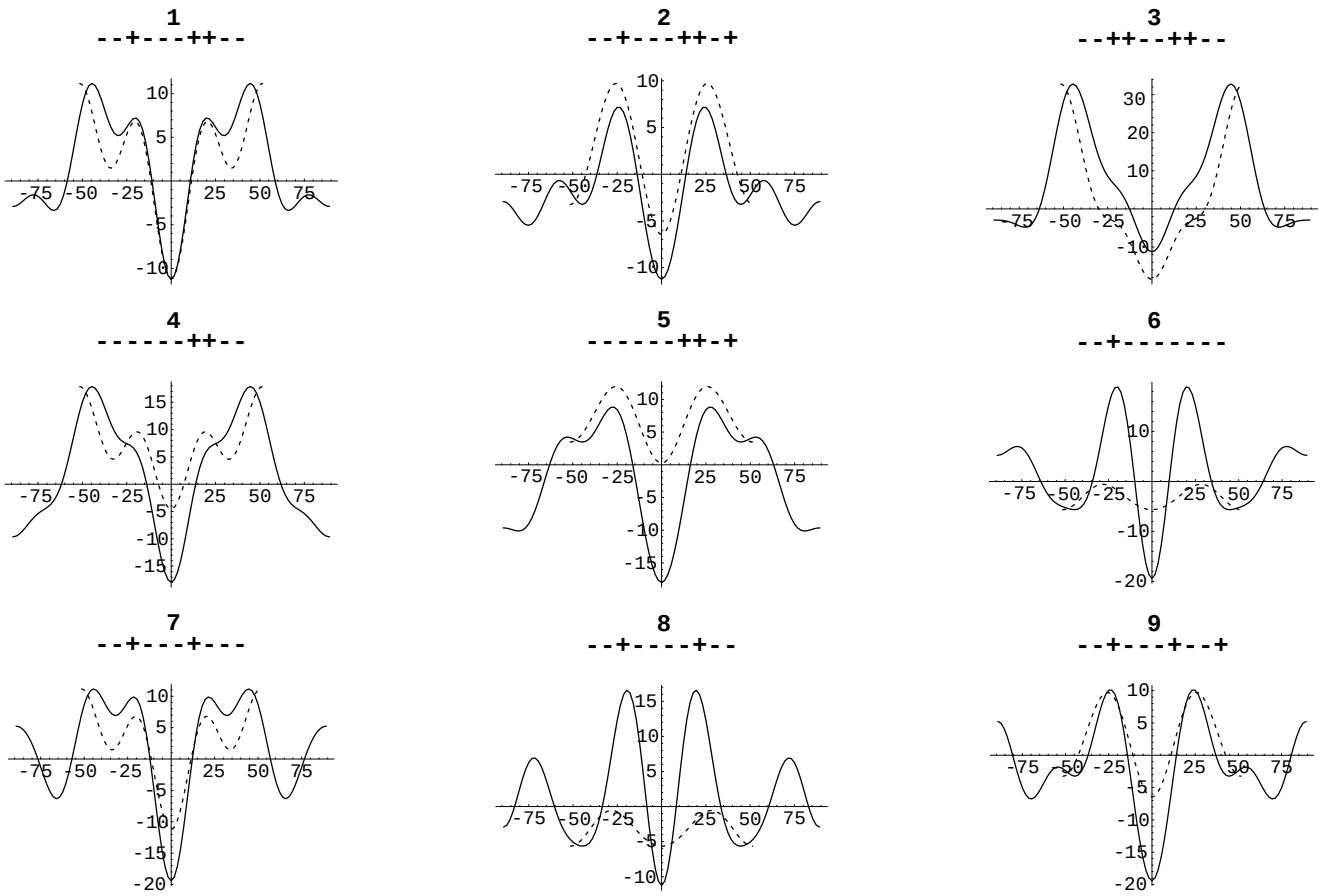

Fig. 6. Electron density cuts for the top nine phasings of modeled mono-olein data. For the phasing at the top of each plot, the solid and dashed lines are perpendicular cuts through the bilayer at the flat point and at a point of maximum curvature. The x-axes are in Angstroms and the y-axes are in arbitrary units.

known from bilayer electron density reconstructions. One can make sense of this if one recalls the results of [29], in which it was noted that reconstructions of the D surface based phases retain artifacts in the water region. Another point worth mentioning is that in the mono-olein system, it is the methyl trough that offers the most contrast. In a phospholipid system, the high electron density phosphorous headgroups offer as much contrast as the methyl groups, and the artifacts in the water region are much reduced (see section 9 for a more thorough discussion of this point). Finally, it is worth reiterating that when one observes diffraction from a system like mono-olein, one primarily observes the methyl trough. This is a disadvantage in investigating the headgroup-water interface, but an advantage in probing the state of the ends of the lipid tails.

From the diagrams of the electron density cuts (top nine shown in Fig. 6) one can eliminate the phasings ranked two, four through six, eight through fourteen, sixteen, and seventeen, on the grounds that the electron density in the water region dips below the methyl trough of at least one of the cuts. The phasings ranked three and fifteen can be eliminated by the following reasoning: the methyl trough should be the dominant feature, being quite deep with lesser variations present in the headgroup and water regions. In these two phasings the greatest variation is in the headgroup and water regions, with the methyl trough a comparatively minor feature, and so these phase combinations are rejected. This leaves the phasings ranked one and seven. *A priori*, it would be difficult to choose between them from the cuts. However, as phasing one has $\Delta_{\max} = 0.0004$, which is much less than phasing number seven ($\Delta_{\max} = 0.0316$), the balance is tipped in favor of the proper phasing, number one ($- - + - - - + + - -$), which is the same as for the phospholipid system discussed in the next section. Thus, the methyl trough search method identifies the correct phasing of a model system from the simulated amplitudes alone.

8 Reconstruction of a model phospholipid system

Here the methyl trough search method is tested by using it to reconstruct the model of a phospholipid D surface based system from section 3.2 of [29]. The amplitudes are listed in Table 3 and the results of the methyl trough search are listed in Table 4. Also listed in the same table are the model amplitudes with noise added. Random (white) noise from 0-10% of the first peak amplitude was added or subtracted from each of the model amplitudes. Given that the first peak was normalized to 1, this means that a random value from -0.1 to $+0.1$ was added to each peak amplitude. The resulting amplitudes were then renormalized to the new value of the first-order peak. For example, if the new value of the first peak was 1.05 after the noise was added in, all the peaks were divided by 1.05. Note that the renormalization has no effect on the phasing process; it was only performed to preserve the custom that is maintained throughout the entire paper of normalizing to the first peak. Satisfyingly, the correct phasing pops up close to the top of each of the phase rankings, with the methyl trough search surface of the correct phasing in good agreement with the minimal surface. As noted earlier, the correct phasing is that for which $\Delta_{\max} < 0.1$ and there are over fifty phasings that satisfy this criterion and many match the minimal surface quite well.

Table 3. Model amplitudes for a phospholipid, D surface based structure. Also shown are amplitudes with noise added in. See text for further explanation.

q	Phospholipid model	
		(w/noise)
$(1,1,0)$	-1.00	-1.00
$(1,1,1)$	-1.12	-1.17
$(2,0,0)$	$+0.71$	$+0.78$
$(2,1,1)$	-0.59	-0.57
$(2,2,0)$	-0.67	-0.56
$(2,2,1)$	-0.69	-0.68
$(3,1,0)$	$+0.38$	$+0.30$
$(3,1,1)$	$+0.17$	$+0.17$
$(2,2,2)$	-0.53	-0.54
$(3,2,1)$	-0.12	-0.21
$(4,0,0)$	-0.08	-0.08
$(3,2,2)$	-0.08	-0.10

From the electron density cuts displayed in the correct phasing ranked 3 of Figure 7 for the model system, intuition can be gained on what one expects to see in a reconstruction of a phospholipid system at this resolution. Working from the center out, one sees, as expected, a deep trough in the center due to the terminal methyls and the remainder of the hydrocarbon tails. Next, on both sides of the trough, note the peaks due to the phosphorous-dominated headgroups. Finally, in the water region outside the bilayer, note the small peaks that are truncation artifacts. These are reminiscent of the bump one sees in the center of a reconstruction of the H_{II} phase [27]. At the risk of oversimplification, one might say that since the electron density of the water region is flat, this is precisely the region in which one would expect to see the wiggles and bumps of truncation effects. In short, flat regions are poorly represented by only a few terms of a Fourier expansion. Also of note is that the troughs and headgroup peaks for the two cuts overlay very well for the model, with the headgroup peak for the cut through maximum curvature region being moved only slightly out from the headgroup peak for the cut through the flat point, offering encouragement for eventually examining thickness variations in the bilayer. The small offset that does exist is due to the fact that the surface defined by the headgroups bends *away* from the minimal surface at the cut at maximum curvature, thus pulling the maxima away as well. It is interesting, and comforting, to note that the truncation artifacts do not overlay well; again, at the risk of oversimplification, it might be said that those aspects of the reconstruction which are real are robust and that those

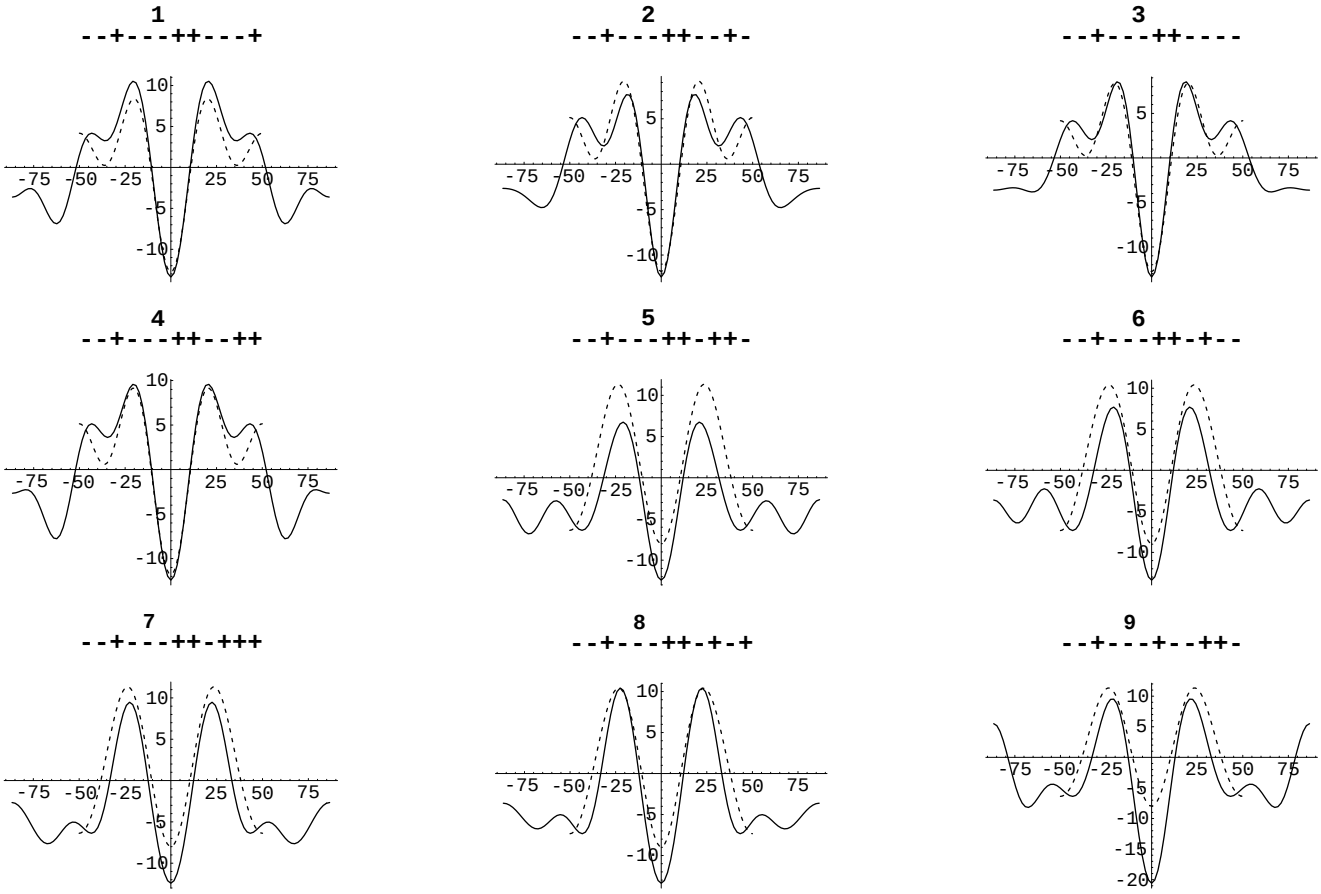

Fig. 7. Electron density cuts for the top nine phasings of modeled phospholipid data. For the phasing at the top of each plot, the solid and dashed lines are perpendicular cuts through the bilayer at the flat point and at a point of maximum curvature. The x-axes are in Angstroms and the y-axes are in arbitrary units.

which are artifacts are highly variable. Also note that it is fortunate to have headgroups with a high electron density that dominates over the artifacts; there is not such an advantage in studying mono-olein, which presented some difficulty in interpreting the cuts. Finally, note that despite truncation artifacts, the average electron density in the water region lies comfortably in between the electron densities for the methyl troughs and phosphorous peaks, as expected. Furthermore, the artifacts in the water region stay well below the headgroup peak and well above the methyl trough.

With this insight into what a reconstruction should look like, the top phasings for the model can be sorted through and some constraints developed to select the proper phasing from the remaining combinations. Properly, one examines the cuts for all fifty or so phasings that satisfy the criterion that $\Delta_{\max} < 0.1$. As this would take overly long, only the first nine will be explicitly examined; a similar examination would suffice for the remainder of the phasings. Furthermore, it is noted that for experimental data only a dozen or so phasings satisfy the criterion $\Delta_{\max} < 0.1$; for the experimental data all the phasings that satisfy this criterion will be explicitly examined.

The cuts displayed for the top nine phasings from the methyl trough search are displayed in Figure 7. For phasings ranked five through nine, the average electron density in the water region is roughly equal to the trough electron density for the cut through the point of maximum curvature. As this is unphysical, these phasings can be readily eliminated. The remainder of the phasing combinations all yield similar results and there does not seem to be grounds for definitively choosing one and eliminating the others. However, the phasing ranked three has the smoothest water region and the shallowest dips in that region, earning it the distinction of the most favored phasing among the top four candidates. This is a good example of the need to examine the electron density cuts. The criterion $\Delta_{\max} < 0.1$ is a good way to reduce the set of acceptable phasing combinations to a reasonable number; however, it is unwise to use the $\Delta_{\max}$ value as the sole criterion for picking the best phasing.

9 Truncation effects and headgroup variation

As a test of the robustness of the methyl trough phasing method under truncation, it is used to phase the first three and first seven peaks of the phospholipid model. Pleasingly, the correct phasing is ranked number one in both phase lists. For the three peak truncation, only the first

Table 4. Methyl trough phasing results for the top ranked phasings for a model phospholipid system. The correct phasing is marked with an arrow.

Rank	$\Delta_{\max}$	Δ_{rms}	Phasing											
			1	1	2	2	2	2	3	3	2	3	4	3
			1	1	0	1	2	2	1	1	2	2	0	2
			0	1	0	1	0	1	0	1	2	1	0	2
1	0.0003	0.0001	−	−	+	−	−	−	+	+	−	−	−	+
2	0.0014	0.0006	−	−	+	−	−	−	+	+	−	−	+	−
3	0.0022	0.0009	−	−	+	−	−	−	+	+	−	−	−	− ⇐
4	0.0043	0.0018	−	−	+	−	−	−	+	+	−	−	+	+
5	0.0097	0.0056	−	−	+	−	−	−	+	+	−	+	+	−
6	0.0115	0.0052	−	−	+	−	−	−	+	+	−	+	−	−
7	0.0140	0.0074	−	−	+	−	−	−	+	+	−	+	+	+
8	0.0141	0.0069	−	−	+	−	−	−	+	+	−	+	−	+
9	0.0202	0.0087	−	−	+	−	−	−	+	−	−	+	+	−

phasing satisfies the criterion $\Delta_{\max} < 0.1$ and so the remaining phasings do not require further examination. For the seven peak truncation, the top three phasings satisfy the above criterion. Phasings ranked two and three suffer from the defect that the electron density in the water region dips below the methyl trough electron density, which is unphysical (plots not shown). Therefore, the only satisfactory phasing is the phasing ranked number one, which is the correct phasing for the model.

As noted in [29] and in previous sections in this paper, a difficulty in reconstructing D surface based phases is the existence of strong truncation artifacts in the water region of the reconstruction. These artifacts are more prominent in reconstructing system with a low headgroup electron density, such as mono-olein, than in a system with a high headgroup electron density, like a phospholipid system. Indeed, this effect can be clearly displayed if the phospholipid model (section 3.2 of [29]) is considered and the headgroup electron density is reduced to that of mono-olein (section 6). In Figure 8, the electron density cuts are plotted for reconstructions of models in which the headgroup electron density has been smoothly varied from that of a phospholipid to that of mono-olein. As can be seen, the artifacts in the water region are subordinate to the headgroup peaks when the headgroup electron densities are equal to phospholipid levels. When the headgroup electron densities are reduced to mono-olein levels, the artifacts dominate over the headgroup peaks.

10 Reconstruction of mono-olein

Having now shown that the methyl trough search method may be used to correctly phase model data, we turn to phasing real experimental data. The amplitude data for mono-olein for the experiments of [13,14], this work, and for the model constructed in [29] are listed in Table 5. The mono-olein data was taken by the methods described in section 1 and a graph of the data is shown in Figure 1. Defining resolution as in [35], one has

$$\Delta r = \frac{1.22a}{q_{\max}}, \tag{15}$$

where a is the unit cell size and $q_{\max}$ is the maximum reciprocal space vector. For my mono-olein data, $a = 103\,\text{Å}$ and $q_{\max} = \sqrt{14}$, and so $\Delta r = 38\,\text{Å}$. The resolution for the other data sets is roughly the same. Both the apodized and unaltered amplitudes from Mariani *et al.* [14] are used. (See section 4 for a description of apodization.) A β of $462\,\text{Å}^2$ was used by Mariani *et al.* [14] for this data. There is a fair amount of variation in the amplitudes; it is not entirely clear whether this is due to experimental error or real variation in the structure of mono-olein at the different d-spacings. A calculation was made of how the amplitudes would change with a 10% change in d-spacing in the model data; the small variation was insufficient to explain the variation in the data sets. It is worth noting that the background is not insubstantial (see Fig. 1), which is common to all the $\mathrm{Pn\bar{3}m}$ diffraction patterns we have seen. Neither [14] or [13] mention any effort to fit or otherwise account for background scattering. However, it should be noted that mono-olein phase behavior is quite hysteretic in this region of its phase diagram and the variation in d-spacings is quite reasonable. For a quantitative index of this match up of the amplitudes, define an R factor, or figure of merit, which is

$$R = \frac{\sum_{hkl}(|F_{hkl}^{\mathrm{obs}}| - +|F_{hkl}^{\mathrm{model}}|^2)}{\sum_{\mathrm{hkl}}(F_{hkl}^{\mathrm{obs}})^2}, \tag{16}$$

where F_{ijk}^{obs} are the observable amplitudes and F_{ijk}^{calc} are the model amplitudes. As can be seen, the data of Longley and McIntosh [13] (see Tab. 5) differ from the model more than the other sets. However, despite the variations in the amplitudes, the phasing results remain practically the same for each of the systems, as will be shown.

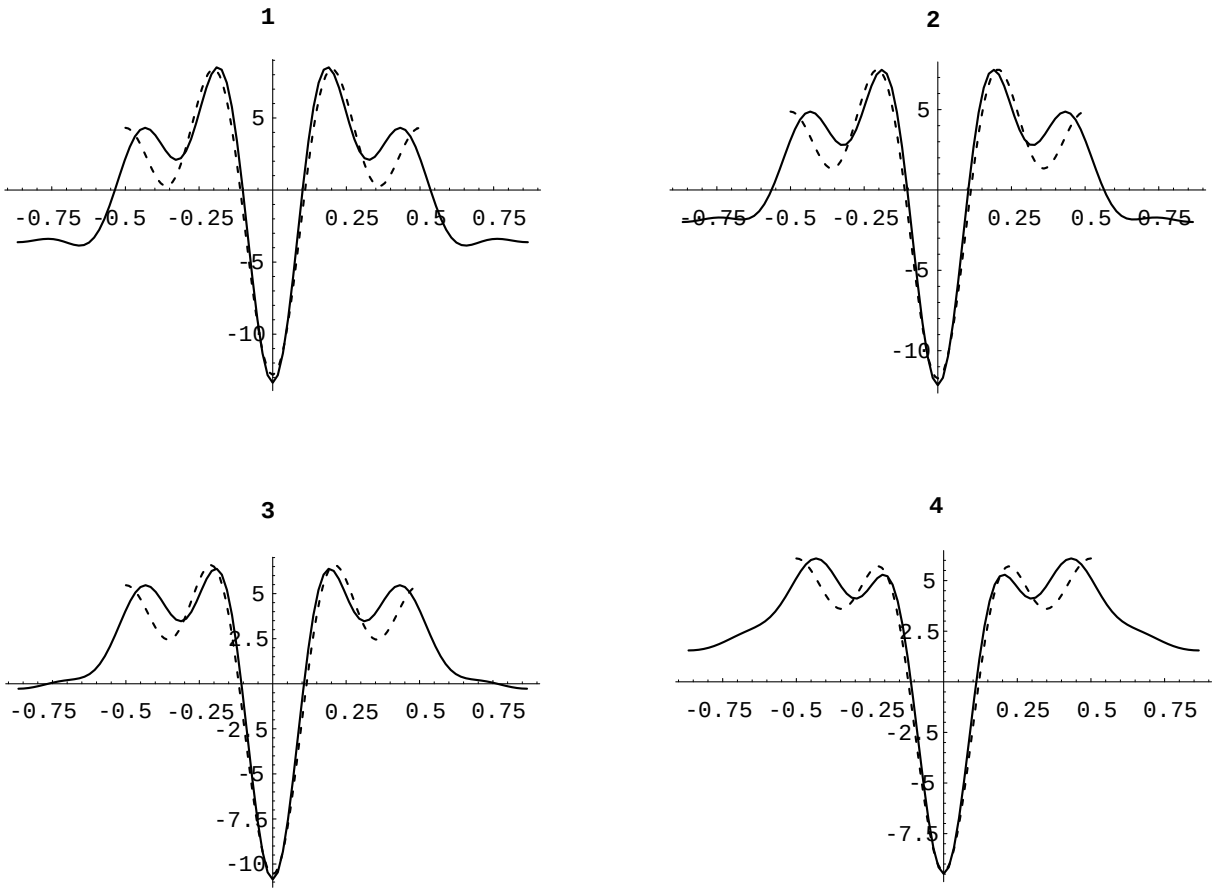

Fig. 8. Plot number 1 contains the electron density cuts for the phospholipid model. Plot number 4 contains the electron density cuts for the same model, except that the headgroup electron density used is from the mono-olein model. Plots 2 and 3 are plots of the electron density cuts for intermediate headgroup electron densities. The x-axes are in Angstroms and the y-axes are in arbitrary units.

Table 5. Experimental and model amplitudes for mono-olein. The R factor is calculated relative to the model. See the text for an explanation of the apodized and non-apodized amplitudes for [14]. The amplitude modulus is given for the experimental data, whereas the model also has the appropriate sign.

	Longley [13]	Mariani [14]		This work	Model
		(apodization)	(no apodization)		
T (°C)	22	25		25	—
d-spacing (Å)	105	96.4		103	—
R	0.120	0.027	0.048	0.037	—
q					
$(1,1,0)$	1.00	1.00	1.00	1.00	−1.00
$(1,1,1)$	1.17	0.96	1.01	0.96	−1.03
$(2,0,0)$	0.69	0.75	0.82	0.54	+0.56
$(2,1,1)$	0.60	0.42	0.51	0.35	−0.45
$(2,2,0)$	0.99	0.46	0.63	0.47	−0.53
$(2,2,1)$	0.67	0.45	0.64	0.42	−0.56
$(3,1,0)$	0.32	0.37	0.55	0.22	+0.35
$(3,1,1)$	0.21	—	—	—	+0.17
$(2,2,2)$	—	0.44	0.72	0.19	−0.51
$(3,2,1)$	—	0.17	0.30	0.0	−0.15

Table 6. Top ranked methyl trough phasing results for mono-olein data from this work. The best phasing is marked with an arrow.

Rank	$\Delta_{\max}$	Δ_{rms}	Phasing											
			1	1	2	2	2	2	3	3	2	3	4	3
			1	1	0	1	2	2	1	1	2	2	0	2
			0	1	0	1	0	1	0	1	2	1	0	2
1	0.0114	0.0047	−	−	+	−	−	−	+	0	−	0	0	0 ⇐
2	0.0114	0.0047	−	−	+	−	−	−	+	0	+	0	0	0
3	0.0487	0.0225	−	−	+	+	−	−	+	0	−	0	0	0
4	0.0487	0.0225	−	−	+	+	−	−	+	0	+	0	0	0
5	0.0489	0.0212	−	−	−	−	−	−	+	0	−	0	0	0
6	0.0489	0.0212	−	−	−	−	−	−	+	0	+	0	0	0
7	0.0802	0.0419	−	−	−	+	−	−	+	0	−	0	0	0
8	0.1519	0.0651	−	−	+	−	+	−	+	0	−	0	0	0
9	0.1519	0.0875	−	−	+	−	+	+	+	0	−	0	0	0

Using the phasing $(--++++--)$ of Longley and McIntosh [13] results in a greatly distorted methyl trough surface. If a methyl trough search is performed using the amplitudes of Longley and McIntosh, one finds that their phasing ranks number 94 out of 256, with a $\Delta_{\max} = 0.5$, well in excess of the cut off of $\Delta_{\max} < 0.1$, and so this phasing is rejected, as have [14]. A factor in the incorrect phasing of [13] is that the structure was mistakenly assumed to be a type-I phase; *i.e.*, their model has lipids where there should be water and vice versa. The amplitudes of the Longley and McIntosh data are used for a methyl trough search and only the top five satisfy $\Delta_{\max} < 0.1$. The electron density cuts can then be used to pick the best phasing from among these five. All but the phasing ranked number four $(--+---+-)$ have the difficulty that the electron density in the water region dips to or below the electron density of the methyl trough. This phasing is identical to that of the model, except for the final peak. Interestingly, that same peak is not seen in either the data of Mariani *et al.* [14] or ours. It is also noted that the headgroup peaks do not overlay as well as in the model system and that the water region is rather different than in the model system. However, as the water region is artifact dominated, this is not a major point (see section 9).

Now move on to a consideration of both the apodized and unaltered amplitudes from Mariani *et al.* [14] (see Tab. 5). As the apodized amplitudes are the ones used in [14] for reconstruction, these will be considered first; we then consider the unaltered amplitudes. A methyl trough search on the apodized amplitudes yields fourteen phasings that satisfy the $\Delta_{\max} < 0.1$ criterion. Of these, all but three combinations can be eliminated as in the remainder the electron density in the water region drops to or below the electron density for the methyl trough. Of these, one can be eliminated by the following rationale: The headgroup peak separation should correspond roughly to the bilayer thickness. In this combination, the bilayer peak separation is roughly one unit cell, which would correspond to 96 Å. As this is at least twice the thickness of a mono-olein bilayer, this phasing can be discounted. The remaining two phasings present a more difficult choice. However, the top ranked phasing yields a result much more in congruence with the modeling results. Furthermore, the following argument can be made: after averaging out artifacts in the water region, the dominant feature of the reconstruction should be the methyl troughs, *i.e.*, the troughs should be deeper than the peaks are high. Additionally, despite artifacts, the methyl troughs should be solidly deeper than the minima in the water region. These points lead us to conclude that the proper phasing is number one, or $--+---+0--$, which is the same as the phasing picked for Longley and McIntosh's data [13] for the peaks that are seen in both data sets. Finally, this phasing is also in complete agreement with Mariani *et al.*'s [14] phasing of $-++--++0--$, as is explained below. Mariani *et al.* [14] chose to work with a unit cell centered on water; in this work it was decided to work with a unit cell centered on the bilayer. The two centers are separated by a translation of half a unit cell or (0.5, 0.5, 0.5). The phasings for unit cells centered on the water and the bilayer are then related by

$$F_{hkl}^{\mathrm{bilayer}} = F_{hkl}^{\mathrm{water}} \times (-1)^{(h+k+l)}, \tag{17}$$

where $F_{hkl}^{\mathrm{bilayer}}$ are the amplitudes for a bilayer centered unit cell, F_{hkl}^{water} are the amplitudes for a water centered unit cell, and hkl are the indices for a given amplitude.

Next, consider the unaltered or un-apodized amplitudes for Mariani *et al.* [14] data. A methyl trough search for these amplitudes yields only two possibilities that satisfy $\Delta_{\max} < 0.1$. By examining the electron density cuts, one can eliminate a phasing combination, as it has minima in the water region that dip below one of the methyl trough minima. The remaining phasing, ranked number one, is $--+---+0--$ or the same as for the apodized data.

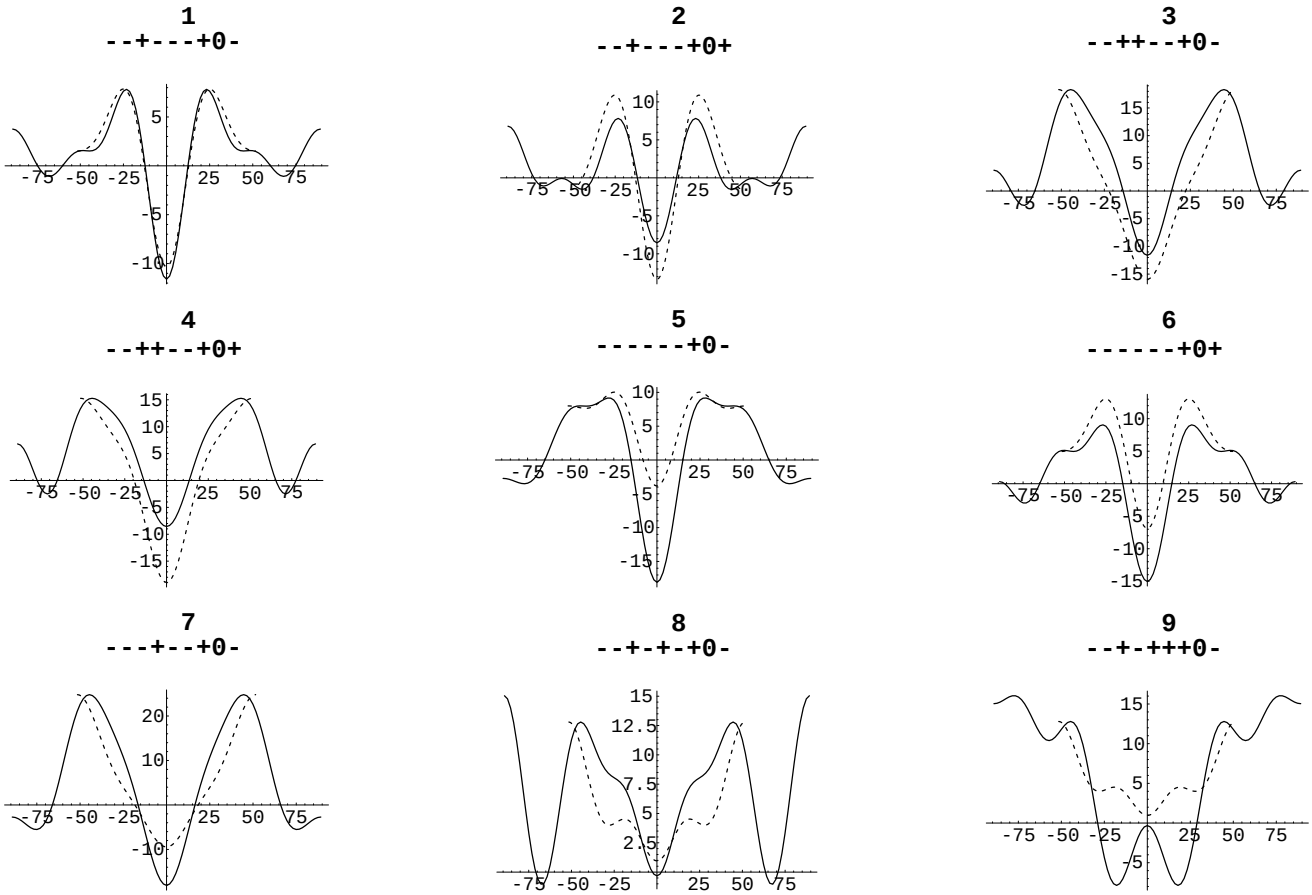

Fig. 9. Electron density cuts for the top nine phasings of mono-olein data from this work. For the phasing at the top of each plot, the solid and dashed lines are perpendicular cuts through the bilayer at the flat point and at a point of maximum curvature, respectively. The x-axes are in Angstroms and the y-axes are in arbitrary units.

Thus far, good agreement has been found in applying the methyl trough search method to both apodized and unaltered data of both [13] and [14] and we derive the same phasing as in [14]. To round out this section, the methyl trough search will be applied to our own data for mono-olein (data shown in Tab. 5.) A methyl trough search results in seven phasings that fit the criterion $\Delta_{\max} < 0.1$ (see Tab. 6). From the electron density cuts for this data (Fig. 9), one sees that the phasings ranked numbered four through seven are disqualified as the electron density in the water region dips below or close to the methyl trough of at least one of the electron density cuts. If one demands, as argued previously, that the dominant feature be the methyl troughs, as well as arguing for the headgroup maxima to overlay, the phasing ranked number one, $(--+---+0-)$, is the best choice, which agrees with the phasing results for the other data sets.

A direct comparison of this reconstruction to the mono-olein model is shown in Figure 10. The methyl trough regions in the center overlap rather well, indicating a fairly uniform state for the methyl tails. The model headgroup peaks are closer together than for the reconstructed data, perhaps indicating that the bilayer is actually thicker than modeled. Also note that the bilayer thickness, as marked by the headgroup peaks, appears to be the same to within a couple of angstroms in both the flat and highly curved region of the bilayer. It is good to reiterate the caution that the main feature of this system is the methyl troughs and that it is dangerous to over interpret the headgroup peaks. Finally, consider the hydrated region outside the bilayers. Here the reconstruction is artifact ridden, as noted earlier (see section 9), and therefore not a very fruitful area for analysis.

11 Reconstruction of a phospholipid system

In this section, the phospholipid 2-2 methyl butyl 16:0 PC is examined. This lipid is one of a new class of non-lamellar forming lipids with PC headgroups [18]. Briefly, it appears that their novel behavior is due to the attachment of hydrocarbon groups to the tails at a location close to the headgroup. The data was taken by the methods described in section 1 and a graph of the data is shown in Figure 2. Using the resolution defined in equation (15), $a = 100\,\text{Å}$, and $q_{\max} = \sqrt{17}$, a resolution of $\Delta r = 29\,\text{Å}$ is found for this data. For the mono-olein data, $a = 103\,\text{Å}$ and $q_{\max} = \sqrt{14}$, and so $\Delta r = 38\,\text{Å}$. In order to form the Pn$\bar{3}$m phase, the sample was heated to 90 °C. It was

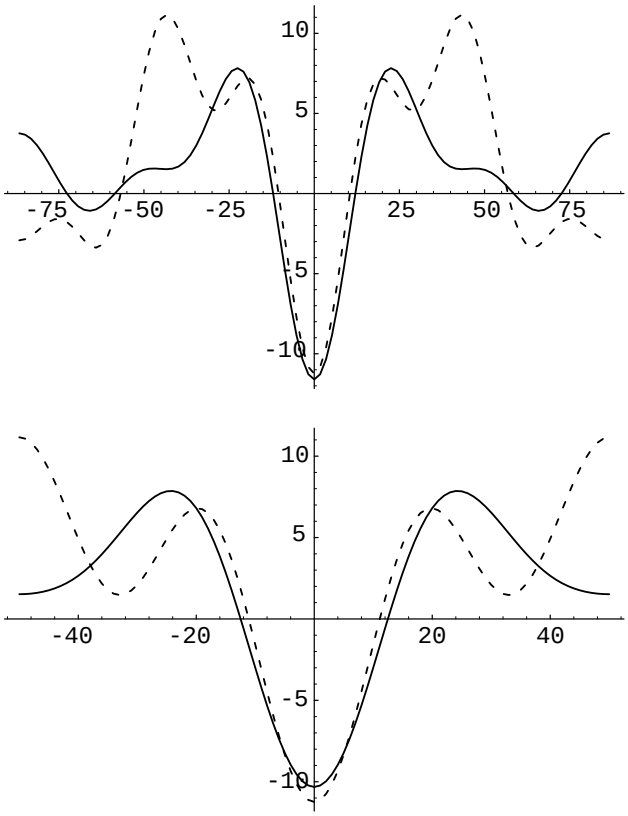

Fig. 10. Data (solid lines) and model (dashed lines) overlay for mono-olein. Top plots: electron density cuts through the flat point. Bottom plots: electron density cuts through the point of maximum curvature.

then cooled to 20 °C, as more orders could be seen at a lower temperature. The analysis is begun by comparing the measured amplitudes for this lipid with those of the phospholipid model (see Tab. 7). Ideally, the model would be tailored for this specific system. Unfortunately, since the quantity of lipid available was small, it was not possible to find the necessary parameters, such as the density of the lipid and the water fraction for this phase, as used in the construction of the mono-olein model. Therefore, it is necessary to use another similar phospholipid, in this case DOPE (dioleoylphosphatidylethanolamine), as a model. See section 3.2 of [29] for details on the construction of a model of DOPE in a D surface based phase. Despite these limitations, one sees that the model amplitudes match up quite well with the measured ones. For this set of experimental and calculated amplitudes one gets a value of $R = 0.01$ (see Eq. (16)).

After executing a methyl trough search (Tab. 8), only the top fourteen phase combinations pass the criterion $\Delta_{\max} < 0.1$. It is also satisfying to note that there is a clear break in the $\Delta_{\max}$ values at this point and that those phasings with $\Delta_{\max} > 0.1$ yield very distorted methyl trough surfaces. The electron density cut plots (Fig. 11, only the top nine phasing combinations are shown) can now be used to pick the best phasing.

Table 7. Experimental amplitudes for 2-2 methyl butyl 16:0 PC at 20 °C in excess water. The d-spacing is 100 Å. Also listed are the amplitudes for a phospholipid model. The determination of the experimental amplitudes is discussed in section 1.

q	2-2 methyl butyl 16:0 PC	Phospholipid model
$(1,1,0)$	1.00	−1.00
$(1,1,1)$	1.17	−1.12
$(2,0,0)$	0.74	+0.71
$(2,1,1)$	0.56	−0.59
$(2,2,0)$	0.71	−0.67
$(2,2,1)$	0.70	−0.69
$(3,1,0)$	0.34	+0.38
$(3,1,1)$	0.00	+0.17
$(2,2,2)$	0.47	−0.53
$(3,2,1)$	0.12	−0.12
$(4,0,0)$	0.00	−0.08
$(3,2,2)$	0.17	−0.08

Phasings ranked 1-4, 7-9, and 11-13 can be eliminated on the grounds that the electron density in the water region dips below the methyl trough for at least one of the cuts. The phasings ranked number ten and fourteen can be ruled out on the following grounds: The distance separating the headgroups gives one at least a first-order estimate of the bilayer thickness. The cuts for these two phasings imply a bilayer thickness of one unit cell, or 100 Å. As this is a factor of two larger than the bilayers produced by lipids of similar chain length, these phasings can be removed from consideration.

At this point, only the phasings ranked five and six remain. Though it is not unreasonable to see some variation between the headgroup electron density peaks at points of different curvature, one does not expect that the integrated electron density peak at one curvature should yield a result roughly twice that at a different curvature. For instance, in a system involving similar stresses on headgroup electron density, the electron density curves were still roughly similar [27]. From this rationale, the phasing ranked six is eliminated and conclude that the phasing number five $(--+---+0--0-)$ is the best choice. Pleasingly, this also matches the phasing of the phospholipid model (see Tab. 7).

As can be seen, electron density cuts are quite similar for the DOPE model and 2-2 methyl butyl 16:0 PC, though there are some differences (see Fig. 12). In passing, it is noted that there are some minor differences in the water region; as this area is artifact dominated, no attempt will be made at interpreting them. Of more interest is the fact that the methyl trough appears to be shallower for the cut through the bilayer at the point of maximum curvature.

Though careful modeling and examination of the effects of disorder are needed to determine whether this is real or not, a possible explanation might be that in the region of high curvature, the region occupied by the methyl

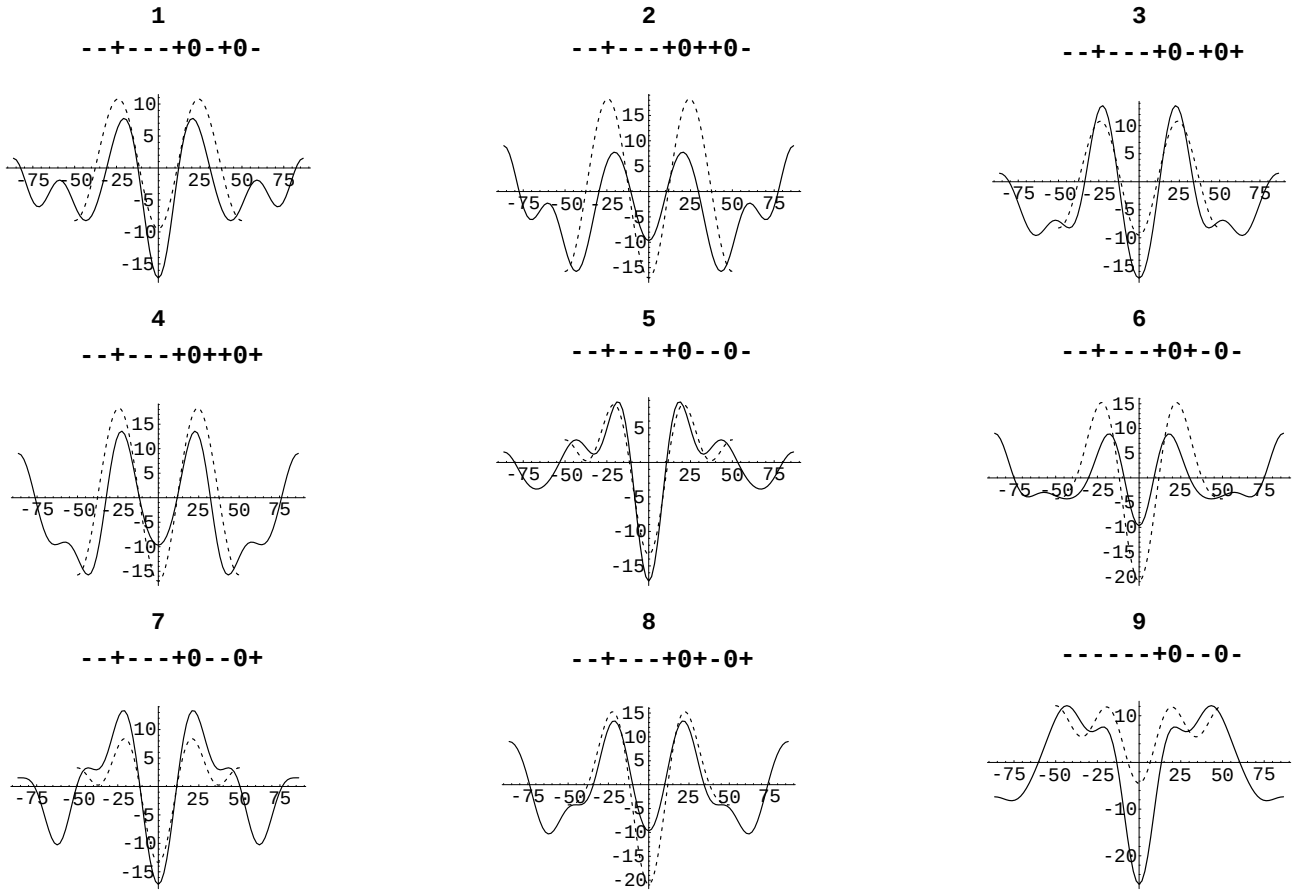

Fig. 11. Electron density cuts for the top nine phasings for 2-2 methyl butyl 16:0 PC. For the phasing at the top of each plot, the solid and dashed lines are perpendicular cuts through the bilayer at the flat point and at a point of maximum curvature. The x-axes are in Angstroms and the y-axes are in arbitrary units.

Table 8. Top ranked methyl trough phasing results for 2-2 methyl butyl 16:0 PC. The best phasing is marked with an arrow.

Rank	$\Delta_{\max}$	Δ_{rms}	Phasing											
			1	1	2	2	2	2	3	3	2	3	4	3
			1	1	0	1	2	2	1	1	2	2	0	2
			0	1	0	1	0	1	0	1	2	1	0	2
1	0.0054	0.0023	−	−	+	−	−	−	+	0	−	+	0	−
2	0.0054	0.0023	−	−	+	−	−	−	+	0	+	+	0	−
3	0.0106	0.0059	−	−	+	−	−	−	+	0	−	+	0	+
4	0.0106	0.0059	−	−	+	−	−	−	+	0	+	+	0	+
5	0.0126	0.0057	−	−	+	−	−	−	+	0	−	−	0	− ⇐
6	0.0126	0.0057	−	−	+	−	−	−	+	0	+	−	0	−
7	0.0182	0.0074	−	−	+	−	−	−	+	0	−	−	0	+
8	0.0182	0.0074	−	−	+	−	−	−	+	0	+	−	0	+
9	0.0371	0.0154	−	−	−	−	−	−	+	0	−	−	0	−

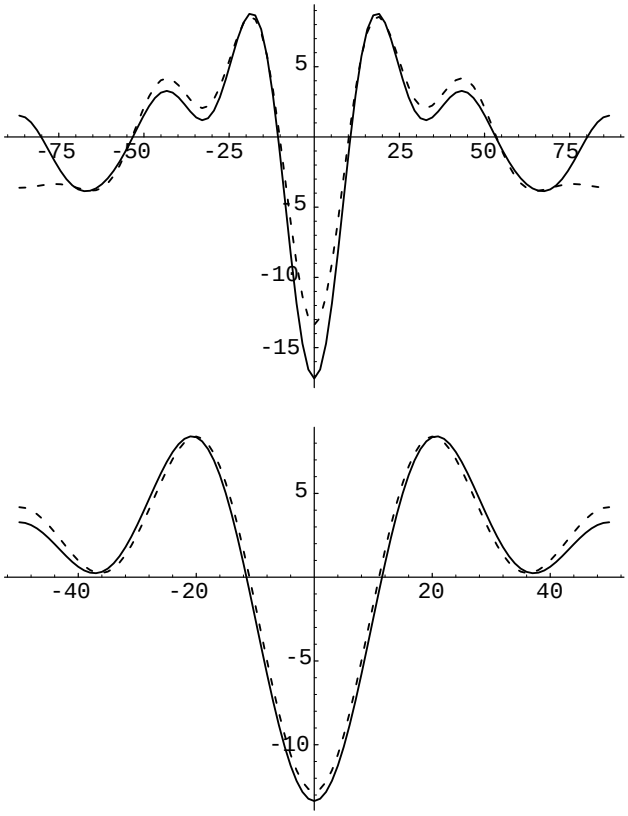

Fig. 12. Data (solid lines) and DOPE model (dashed lines) overlay for 2-2 methyl butyl PC. Top plots: electron density cuts through the flat point. Bottom plots: electron density cuts through the point of maximum curvature.

tails is elongated parallel to the bilayer and hence thinned perpendicular to the bilayer. A low resolution perpendicular cut through the bilayer at this point would sample less of the low density methyls than a cut at a flat point, hence a reduction in the depth of the trough. If this effect is real, it raises the interesting possibility of utilizing IPMS-based reconstructions to examine methyl distributions for a variety of curvatures. Another main feature is the near-perfect overlay of the headgroup peaks for the model and the data. This suggests, with the aforementioned *caveats*, that the bilayer is of uniform thickness, an important point in calculating free energies for the phase.

12 Conclusion

In this paper, a new phasing method for D surface based lipid systems has been developed, the methyl trough search, and tested on model mono-olein and phospholipid systems. The phasing method was shown to be robust under the addition of noise to the model amplitudes and under truncation. Additionally, the examination of the bilayer structure in the reconstructions via cuts through the electron density was shown to be useful in choosing the proper phasing. The methyl trough and headgroup peaks were quite similar at different points in the bilayer; however, the aqueous region of the reconstructions were shown to be prone to truncation artifacts (see section 9). Next, several mono-olein systems were reconstructed from real experimental diffraction amplitudes. As the methyl trough is the dominant feature in a mono-olein–water systems, the methyl trough method worked quite well for these systems. It was found that truncation artifacts in the aqueous region of the reconstruction sometimes overshadowed the low contrast headgroup peaks of this system, a reversal of the situation for the phospholipid system. The methyl trough search was applied to the previous reconstruction efforts of [13,14], as well the mono-olein data taken for this paper. The results were in agreement with [14] and conflicted with [13]. Finally, a phospholipid system, 2-2 methyl butyl 16:0 PC, was reconstructed from experimental amplitudes using the methyl trough search method, and the phasing was shown to be identical to that of the model phospholipid system, as well as the mono-olein systems.

The good match between the modeling and experimental amplitudes lends strong support to the contention that the systems studied are based on minimal systems. Furthermore, the best surface found by the methyl trough search yielded excellent agreement with the actual minimal surface. Even though this was the criterion used for phasing, the fact that such strong congruence existed also adds strength to the conclusion that these structures are indeed based on minimal surfaces.

Suggestively, the bilayer thickness appeared to be the same in the flat and highly curved portions of the system. Indeed, it is clear that a constant thickness model is at least a good first-order description of the actual structure. The next step is to make a detailed examination of thickness variations in the lipid bilayer over the minimal surface. Lipid morphologies appear to be driven by some competition between curvature and chain length energies [11]. If curvature energies are dominant, then a constant curvature surface would result. On the other hand, if chain length energies dominate, a constant thickness surface would be the result. Therefore, it seems reasonable to believe that the lipid-water interface will lie somewhere in between these two extremes and that the position of the interface will yield substantial insight into the nature of these two energies. Since there has not yet been a satisfactory theory that quantitatively describes both the curvature and the chain length energies, a measurement of the interface would be quite important.

As shown in [36], small variations in the thickness of the bilayer in D surface systems separate constant curvature and constant thickness bilayer configurations. An attempt to experimentally measure deviations from the constant thickness structure would require more modeling and a careful consideration of disorder on the peak amplitudes. Though in this paper the methyl trough search is used for D surface based systems, it would be straightforward to apply the technique to G surface based systems. D surface based systems seem to suffer from the large background present in the diffraction data, a feature common to all the diffraction pictures with which the authors are familiar. Though identifying the cause of this back-

ground is an interesting point in and of itself, it would seem much more straightforward to work with a G surface based phase that does not exhibit this problem. Furthermore, low resolution reconstructions of the G surface do not contain the substantial artifacts present in D surface based systems. One drawback to working with the G surface is its higher degree of complexity and the greater calculation effort required. However, with the rapidly increasing amount of computation power available to the average researcher, this is becoming a much less significant difficulty. It therefore seems that an analysis of thickness variations would best be performed with a system based on the G surface.

We are grateful for a National Science Foundation Fellowship and Liposome Co. Fellowship for P.H. and for support from the D.O.E. (grant DE-FG02-87-ER60522).

References

1. L.E. Scriven, Nature (London) **266**, 123 (1976).
2. A. Fogden, S.T. Hyde, Eur. Phys. J. B **7**, 91 (1999).
3. R.H. Templer, Curr. Opin. Colloid In. **3**, 255 (1998).
4. R.H. Templer, J.M. Seddon, N.A. Warrender, A. Syrykh, Z. Huang, R. Winter, J. Erbes, J. Phys. Chem. B **102**, 7251 (1998).
5. R.H. Templer, J.M. Seddon, P.M. Duesing, R. Winter, J. Erbes, J. Phys. Chem. B **102**, 7262 (1998).
6. R.H. Templer, B.J. Khoo, J.M. Seddon, Langmuir **14**, 7427 (1998).
7. J.H. Laurer, D.A. Hajduk, J.C. Fung, J.W. Sedat, S.D. Smith, S.M. Gruner, D.A. Agard, R.J. Spontak, Macromolecules **30**, 3938 (1997).
8. P. Alexandridis, U. Olsson, B. Lindman, Langmuir **14**, 2627 (1998).
9. S. Andersson, S.T. Hyde, K. Larsson, S. Lidin, Chem. Rev. **88**, 221 (1988).
10. W. Helfrich, H. Rennschuh, J. Phys. (Paris) **23**, C7, 189 (1990).
11. D.C. Turner, Z.-G. Wang, S.M. Gruner, D.A. Mannock, R.N. McElhaney, J. Phys. II France **2**, 2039 (1992).
12. R. Templer, D.C. Turner, P. Harper, J.M. Seddon, J. Phys. II France **5**, 1053 (1995).
13. W. Longley, T.J. McIntosh, Nature **303**, 612 (1983).
14. P. Mariani, H. Delacroix, V. Luzzati, J. Mol. Biol. **204**, 165 (1988).
15. V. Luzzati, P. Mariani, H. Delacroix, Makromol. Chem., Macromol. Symp. **15**, 1 (1988).
16. V. Luzzati, R. Vargas, A. Gulik, P. Mariani, J.M. Seddon, E. Rivas, Biochemistry **31**, 279 (1992).
17. P.E. Harper, Ph.D. thesis, Princeton University, 1996.
18. R.N.A.H. Lewis, R.N. McElhaney, P.E. Harper, D.C. Turner, S.M. Gruner, Biophys. J. **66**, 1088 (1994).
19. M.W. Tate, S.M. Gruner, E.F. Eikenberry, Rev. Sci. Instrum. **68**, 47 (1997).
20. S.M. Gruner, J.R. Milch, G.T. Reynolds, Rev. Sci. Instrum. **53**, 1770 (1982).
21. V. Vand, A. Aitken, R.K. Campell, Acta Crystallogr. **2**, 398 (1949).
22. N.F.M Henry, K. Lonsdale (editors), *International Tables for X-ray Crystallography,* Vol. **I** (Kynoch Press, Birmingham England, 1969).
23. R. Vargas, P. Mariani, A. Gulik, V. Luzzati, J. Mol. Biol. **225**, 137 (1992).
24. L. Rilfors, P.O. Eriksson, G. Arvidson, G. Lindblom, Biochemistry **25**, 7702 (1986).
25. G. Lindblom, L. Rilfors, Biochim. Biophys. Acta **988**, 221 (1989).
26. S.T. Hyde, S. Andersson, Z. Kristallogr. **168**, 213 (1984).
27. D.C. Turner, S.M. Gruner, Biochemistry, **31** 1340 (1992).
28. A. Tardieu, Ph.D. thesis, Universite Paris-Sud., 1972.
29. P.E. Harper, S.M. Gruner, this issue, p. 217.
30. R.H. Templer, Curr. Opin. Colliod In. **3**, 255 (1998).
31. B.E. Warren, *X-Ray Diffraction* (Addison-Wesley, Reading, MA, 1969).
32. P. Mariani, E. Rivas, V. Luzzati, H. Delacroix, Biochemistry **29**, 6799 (1990).
33. R.C. Weast (editor), *CRC Handbook of Chemistry and Physics*, 55th edn. (CRC Press, Cleveland, OH., 1974).
34. P.T.C. So, Ph.D. thesis, Princeton University, 1992.
35. D.C. Turner, Ph.D. thesis, Princeton University, 1990.
36. D.M. Anderson, S.M. Gruner, S. Leibler, Proc. Natl. Acad. Sci. USA **85**, 5364 (1988).